Research Square

Preprints are preliminary reports that have not undergone peer review.
They should not be considered conclusive, used to inform clinical practice,
or referenced by the media as validated information.

Cross-scale chlorophyll-a monitoring in a canyon-type reservoir using Sentinel-2 and UAV hyperspectral observations

Miaohua Zhong
Fuzhou University
Chaojun Lin
Fuzhou University
Xuewen Chen
Fuzhou University
Lvxin Qian
Fuzhou University
Qiuting Zhang
Longyan Shuifa Environmental Group Co., Ltd
Fan Zhang
Longyan Shuifa Environmental Group Co., Ltd
Kaixin Qiu
Longyan Shuifa Environmental Group Co., Ltd
Wenbin Pan
wenbinpan@fzu.edu.cn

Fuzhou University

Research Article

Keywords: Water quality, reservoir monitoring, spatial heterogeneity, machine learning, multi-platform observation

Posted Date: November 12th, 2026

DOI: https://doi.org/10.21203/rs.3.rs-11488811/v1

License: This work is licensed under a Creative Commons Attribution 4.0 International License.
Read Full License

Additional Declarations: No competing interests reported.

Cross-scale chlorophyll-a monitoring in a canyon-type reservoir using Sentinel-2 and UAV hyperspectral observations

Author(s): Miaohua Zhong[1], Chaojun Lin[1], Xuewen Chen[1], Lvxin Qian[1], Qiuting Zhang[2], Fan Zhang[2], Kaixin Qiu[2], Wenbin Pan[1]

Affiliation(s):

1. School of Environment and Safety Engineering, Fuzhou University, Fuzhou, China

2. Longyan Shuifa Environmental Group Co., Ltd., Longyan, China

Corresponding author: Wenbin Pan

E-mail:

Miaohua Zhong: 240627079@fzu.edu.cn

Chaojun Lin: 230627044@fzu.edu.cn

Xuewen Chen: 240627031@fzu.edu.cn

Lvxin Qian: 240627064@fzu.edu.cn

Qiuting Zhang: 1217255585@qq.com

Fan Zhang: 473212012@qq.com

Kaixin Qiu: kaixinxmu@163.com

Wenbin Pan: wenbinpan@fzu.edu.cn

ORCID:

Acknowledgments

The authors thank Longyan Shuifa Environmental Development Co., Ltd. and Longyan Longjin Environmental Testing Co., Ltd. for field coordination and monitoring support.

Abstract

Monitoring chlorophyll-a (Chl-a) in morphologically complex reservoirs requires observations capable of capturing both reservoir-wide spatial patterns and fine-scale local variability. This study developed a cross-scale Sentinel-2–unmanned aerial vehicle (UAV) framework for Chl-a monitoring in Mianhuatan Reservoir, a canyon-type reservoir in southeastern China. Five field campaigns were conducted between July and October 2025, and field-measured Chl-a concentrations were matched

independently with Sentinel-2 multispectral imagery and UAV hyperspectral observations. After quality control and spatial matching, 150 Sentinel-2–field samples and 47 UAV–field samples were retained for model development. Partial least squares regression, random forest, extreme gradient boosting, and support vector regression were evaluated separately for the two remote-sensing platforms using leave-one-out cross-validation. The optimal UAV support vector regression model achieved an R^2 of 0.81 and an RMSE of 4.72 μg L^{-1}, whereas the optimal Sentinel-2 XGBoost model achieved an R^2 of 0.65 and an RMSE of 5.93 μg L^{-1}. Sentinel-2 provided the reservoir-wide spatial background of Chl-a and revealed broad differences among reservoir sections, while UAV hyperspectral imagery resolved continuous concentration gradients and finer spatial heterogeneity within representative local waters. Under partial cloud-cover conditions, same-day UAV observations further provided spatially continuous high-resolution Chl-a information where the spatial completeness of Sentinel-2 retrievals was reduced. Overall, the proposed framework demonstrates the complementary value of Sentinel-2 and UAV observations across spatial scales and observation conditions. Rather than directly fusing the two products, the framework links reservoir-wide satellite monitoring with targeted UAV-based fine-scale characterization, providing a practical approach for multi-scale Chl-a monitoring in morphologically complex reservoirs.

Keywords

Water quality; reservoir monitoring; spatial heterogeneity; machine learning; multi-platform observation

Introduction

Large canyon-type reservoirs are generally characterized by elongated water bodies, highly developed tributary arms, irregular shorelines, and complex aquatic morphology, while also playing important roles in water regulation, hydropower generation, and ecosystem maintenance. Owing to the combined effects of tributary inflows, hydrodynamic exchange, water-level regulation, and variations in hydraulic residence time, pronounced differences in water movement and material transport often develop among reservoir sections, tributary arms, and nearshore waters, resulting in spatial heterogeneity characterized by the coexistence of reservoir-scale gradients and localized high-concentration areas (Xiang et al., 2021; Cheng et al., 2019). Chlorophyll-a (Chl-a), an important indicator of phytoplankton biomass and trophic status, provides a direct means of characterizing such spatial variability and the associated patterns of algal growth (Carlson, 1977). For example, Wang et al. (2024) reported relatively

high Chl-a concentrations in upstream waters and nearshore tributary bays of the Shending River backwater area in Danjiangkou Reservoir, indicating that broad spatial gradients and localized algal-enrichment zones can coexist within the same reservoir system. Therefore, how to characterize the reservoir-wide spatial background of Chl-a while simultaneously resolving fine-scale heterogeneity within representative local waters remains an important challenge for remote sensing of complex canyon-type reservoirs.

Conventional water-quality monitoring relies primarily on field sampling and laboratory analysis, which provide reliable measurements but are inherently limited in spatial coverage and sampling frequency. Remote sensing offers an effective complement by enabling synoptic and repeated observations of inland waters over large areas (Palmer et al., 2015; Tyler et al., 2016; Gholizadeh et al., 2016). Sentinel-2, in particular, has been widely applied to Chl-a monitoring because its multispectral configuration, 10–20 m spatial resolution, and frequent revisit provide a suitable balance between spatial detail and temporal coverage (Drusch et al., 2012; Toming et al., 2016; Pahlevan et al., 2020; Mamun et al., 2024; Zhao et al., 2024). However, Chl-a retrieval in optically complex inland waters remains challenging (Odermatt et al., 2012; Llodrà-Llabrés et al., 2023). In narrow reservoir branches and nearshore waters, mixed pixels and adjacency effects can contaminate the water-leaving signal (Warren et al., 2019; Wu et al., 2024), while clouds and cloud shadows can further reduce the availability of valid observations (Llodrà-Llabrés et al., 2023). Consequently, although Sentinel-2 is well suited for characterizing reservoir-scale patterns, its ability to resolve fine-scale Chl-a variability in spatially complex waters remains limited.

Unmanned aerial vehicles (UAVs) have emerged as an important platform for high-resolution monitoring of inland waters (Kislik et al., 2018; Wasehun et al., 2024; Liu et al., 2025). Equipped with multispectral or hyperspectral sensors, UAVs can acquire centimeter- to decimeter-scale imagery and capture spectral information related to optically active water-quality parameters, including Chl-a (Gai et al., 2020; Dronova et al., 2021). Their flexible flight planning and high spatial resolution make them particularly suitable for resolving fine-scale features such as nearshore gradients, localized algal accumulations, and spatial variability within narrow or morphologically complex water bodies. However, UAV observations are constrained by limited flight endurance, relatively small spatial coverage, and sensitivity to illumination and environmental conditions, which restrict their application for routine

monitoring over extensive reservoir areas (Ryu, 2022).

Previous studies have investigated Chl-a monitoring using satellite, UAV, and multi-platform remote-sensing approaches. Nguyen et al. (2021) used Sentinel-2 MSI imagery and multiple machine-learning models to retrieve Chl-a in the Tri An Reservoir, demonstrating the feasibility of satellite-based machine learning for reservoir-scale Chl-a monitoring. Lu et al. (2021) compared several machine-learning algorithms using UAV-borne hyperspectral imagery and generated high-resolution Chl-a maps, highlighting the capability of UAV observations for fine-scale water-quality mapping. Cillero Castro et al. (2020) combined Sentinel-2, Landsat 8, and UAV multispectral imagery for eutrophication monitoring in a small reservoir, demonstrating the feasibility of multi-platform observations across spatial resolutions. More recently, Miliutina et al. (2026) integrated ASV-based in situ measurements with UAV multispectral imaging and compared the resulting maps with Sentinel-2 and Landsat products, showing that UAV observations can resolve nearshore gradients and local spatial structures that are less apparent in satellite imagery. However, existing multi-platform studies have mainly focused on retrieval performance, inter-sensor comparison, or demonstrations at individual spatial scales, while the functional coordination of satellite and UAV observations across scales remains less clearly defined, particularly for large and morphologically complex reservoirs and under incomplete satellite coverage (Mamun et al., 2024; Wasehun et al., 2025; Zhao et al., 2024).

This study aims to develop and evaluate a cross-scale Sentinel-2–UAV framework for Chl-a monitoring in Mianhuatan Reservoir, a canyon-type reservoir in southeastern China. Field-measured Chl-a concentrations were used as ground-reference data, while Sentinel-2 MSI imagery provided reservoir-wide observations and UAV hyperspectral imagery was acquired over representative local areas. Multiple regression algorithms were developed and evaluated separately for Sentinel-2 and UAV observations to identify the best-performing Chl-a retrieval models. The selected models were then applied to generate Chl-a distribution maps at different spatial scales. The framework was used to characterize the reservoir-wide Chl-a spatial background with Sentinel-2, resolve fine-scale variability within representative local waters using UAV observations, and examine the supplementary role of UAV observations where local cloud contamination limited valid Sentinel-2 retrievals. Through this design, the study evaluates the potential of Sentinel-2 and UAV observations to provide complementary Chl-a information across spatial scales and observation conditions.

Materials and methods

The overall methodological framework adopted in this study is illustrated in Fig. 1. The workflow consisted of five major stages: (1) coordinated multi-platform observations, in which field measurements provided ground-reference Chl-a data, Sentinel-2 MSI imagery provided reservoir-wide observations, and UAV hyperspectral imagery provided high-resolution observations over representative local areas; (2) data preprocessing and spectral feature construction, including Sentinel-2 surface-reflectance preparation and masking, UAV radiometric and geometric correction, image mosaicking, water-body masking, and spatial matching with field measurements; (3) Chl-a retrieval model development, in which multiple regression algorithms were independently constructed for Sentinel-2 and UAV datasets; (4) model evaluation and optimal-model selection based on cross-validated predictions; and (5) spatial mapping and cross-scale analysis, in which the selected models were applied to characterize reservoir-wide Chl-a patterns, local fine-scale spatial heterogeneity, and the supplementary role of UAV observations under incomplete satellite coverage. The following subsections describe each stage in detail.

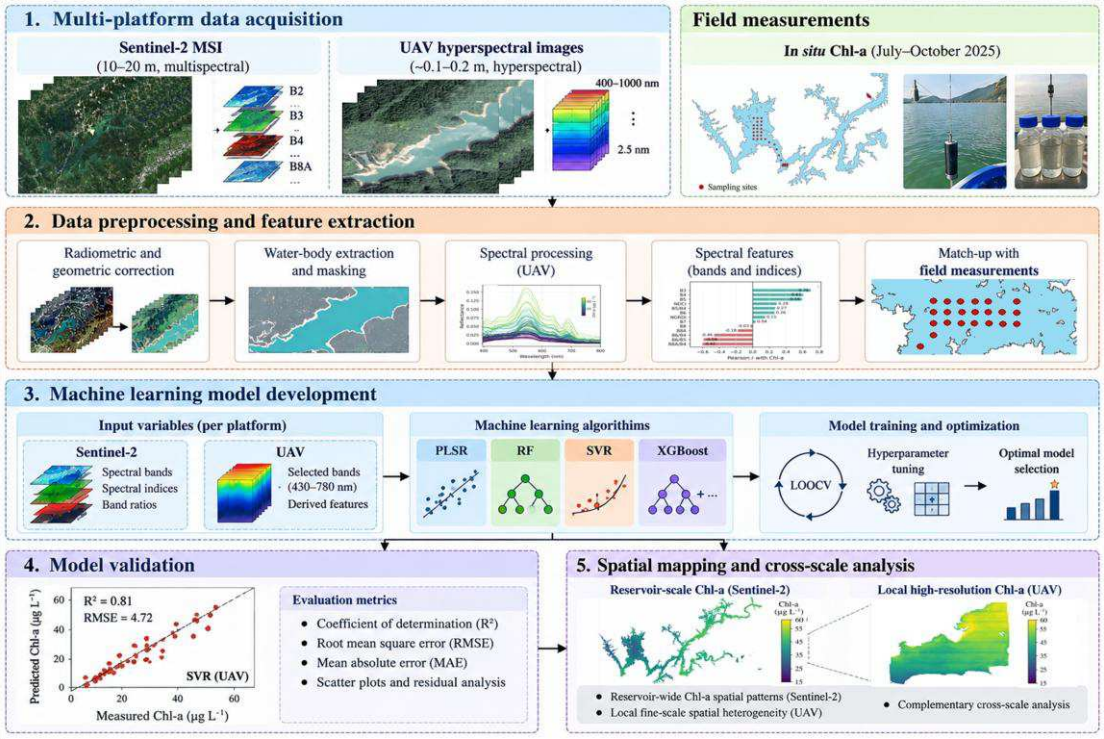


Fig. 1 Workflow of the Sentinel-2–UAV cross-scale Chl-a monitoring framework, including data

acquisition, preprocessing, machine-learning model development, validation, and spatial mapping

Study area

Mianhuatan Reservoir is located in Yongding District, Longyan City, Fujian Province, southeastern China, within approximately 116°23′36″–116°37′24″ E and 24°37′57″–25°02′46″ N (Fig. 2). It is a large canyon-type reservoir formed along the mainstream of the Tingjiang River, with a controlled drainage area of 7907 km², a total storage capacity of 2.035 × 10⁹ m³, and a water surface area of approximately 63 km² at the normal water level. The reservoir is characterized by an elongated main channel, numerous tributary arms, irregular shorelines, nearshore zones, and semi-enclosed bays, resulting in a morphologically complex aquatic environment. These geomorphic characteristics, together with the main–tributary hydrodynamic structure, can contribute to pronounced spatial heterogeneity in water quality. Field sampling sites were distributed across the reservoir, and two representative local areas were selected for UAV hyperspectral surveys to characterize fine-scale Chl-a variability (Fig. 2c–e).

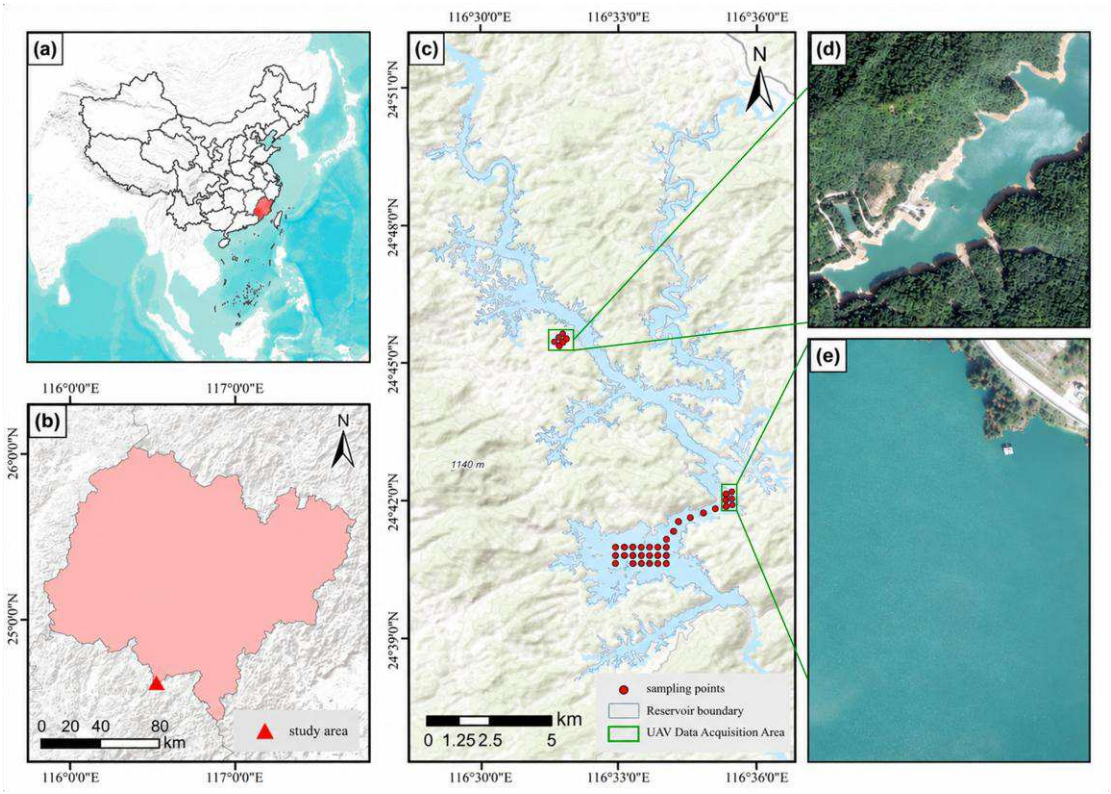


Fig. 2 Study area and survey design. (a) Location of the study area in China (Fujian Province in red); (b) location of the study area within Fujian Province; (c) topography and observation layout of Mianhuatan

Reservoir; (d)–(e) UAV images of typical zones

Multi-platform data acquisition

Field measurements

Five field campaigns were conducted in Mianhuatan Reservoir between July and October 2025, on 1 July, 23 August, 28 August, 17 September, and 7 October. A total of 38 sampling sites were included in each campaign and were distributed mainly across the middle and lower monitoring zones of the reservoir. The sampling locations remained generally consistent among campaigns, and the geographic coordinates of each site were recorded using GPS for subsequent spatial matching with remote-sensing observations.

At each sampling site, surface-water samples were collected at approximately 0.5 m below the water surface using a water sampler. The samples were stored under dark and refrigerated conditions after collection and transported to the laboratory for analysis. Chl-a concentrations were determined using the spectrophotometric method according to the Chinese environmental standard HJ 897-2017 (Ministry of Ecology and Environment of the People's Republic of China, 2017) and were expressed in μg L^{-1}.

Field sampling and UAV hyperspectral surveys were conducted in coordination for each campaign, with UAV acquisition and field sampling completed within approximately 2 h. Sentinel-2 scenes were selected as the nearest suitable observations to the field campaigns, with the acquisition-to-field time difference controlled within ±2 days. This coordinated acquisition strategy minimized temporal mismatch among field, UAV, and satellite observations and reduced uncertainties associated with short-term variations in Chl-a. The observation dates and numbers of sampling sites for each campaign are summarized in Table 1.

Table 1 Summary of field sampling and synchronized UAV–Sentinel-2 observations in Mianhuatan Reservoir

Campaign	Observation date	Sampling sites
1	1 July 2025	38
2	23 August 2025	38
3	28 August 2025	38
4	17 September 2025	38
5	7 October 2025	38

Sentinel-2 imagery

Sentinel-2 Multispectral Instrument (MSI) imagery was used for reservoir-scale Chl-a retrieval and

spatial mapping. The Sentinel-2 MSI acquires data in 13 spectral bands covering the visible, red-edge, near-infrared (NIR), and shortwave-infrared regions, with native spatial resolutions of 10, 20, and 60 m. In this study, harmonized Level-2A surface reflectance products (COPERNICUS/S2_SR_HARMONIZED) were obtained through the Google Earth Engine (GEE) platform (Gorelick et al., 2017). The products provide atmospherically corrected surface reflectance generated using the Sen2Cor processor, with reflectance values stored using a scale factor of 10,000 (Drusch et al., 2012; European Space Agency, 2015; Warren et al., 2019).

Five Sentinel-2 scenes corresponding to the five field campaigns were selected according to the closest suitable acquisition date, with the satellite–field temporal difference controlled within ±2 days. Eight MSI bands relevant to the optical characteristics of inland waters were retained for subsequent Chl-a retrieval: B2 (blue), B3 (green), B4 (red), B5, B6, and B7 (red-edge), B8 (NIR), and B8A (narrow NIR). Among these bands, B2, B3, B4, and B8 have a native spatial resolution of 10 m, whereas B5, B6, B7, and B8A have a native spatial resolution of 20 m. The selected observations were matched to the corresponding field campaigns using the recorded sampling coordinates.

UAV hyperspectral imagery

UAV hyperspectral imagery was acquired using a DJI Matrice 350 RTK platform equipped with an FS60 UAV hyperspectral imaging system (Hangzhou Color Spectrum Technology Co., Ltd., Hangzhou, China). The system integrates hyperspectral data acquisition, wireless image transmission, and GPS–RTK positioning. Under normal RTK operation, the horizontal positioning accuracy can reach 1 cm + 1 ppm, providing sufficient positional accuracy for matching image data with field sampling locations. The hyperspectral sensor covers the 400–1000 nm spectral range with a spectral resolution of 2.5 nm and a signal-to-noise ratio of approximately 600:1.

The UAV was operated at an altitude of approximately 200 m, providing a ground sampling distance (GSD) of 18.83 cm and covering approximately 0.5 km^2 per flight. Flight speed was maintained at approximately 6.2 m s^{-1}, with forward and side overlaps of 80% and 70%, respectively, to ensure sufficient image overlap for subsequent geometric correction and mosaicking. Before each flight, radiometric calibration was performed using a calibrated reflectance reference panel. The UAV was positioned with its nose facing the sun, while the hyperspectral sensor was oriented vertically toward the center of the reference panel to minimize shadow effects and obtain a stable calibration reference. The

panel was subsequently placed on an open and shadow-free surface within the survey area during data acquisition.

UAV surveys were conducted over two representative local areas of Mianhuatan Reservoir to characterize fine-scale spatial variability in Chl-a. UAV acquisition and field sampling were completed within approximately 2 h for each campaign. The survey areas contained both water surfaces and limited shoreline or terrestrial features, which provided spatial reference information for image registration and mosaicking over relatively homogeneous water surfaces. The acquired hyperspectral imagery was subsequently subjected to radiometric correction, geometric correction, mosaicking, water-body masking, and spectral quality control prior to spectral extraction and Chl-a retrieval.

Data preprocessing and feature construction

Because Sentinel-2 MSI and UAV hyperspectral imagery differ substantially in spectral configuration and spatial resolution, the two datasets were processed independently prior to model development.

For Sentinel-2 imagery, the Level-2A surface reflectance data were first scaled using the product scale factor. To ensure spatial consistency among spectral predictors, the native 20 m bands (B5, B6, B7, and B8A) were resampled to the 10 m reference grid using bilinear interpolation, whereas categorical mask data were resampled using the nearest-neighbor method. Cloud and invalid pixels were screened using the Sentinel-2 cloud-probability product (probability < 40%) together with the Scene Classification Layer (SCL), excluding saturated/defective pixels, cloud shadows, medium- and high-probability clouds, cirrus, and snow/ice. NDWI was calculated as (B3 − B8)/(B3 + B8) (McFeeters, 1996; Huang et al., 2018) and used as a water-related spectral feature during quality screening. For field–image matching, a 15 m buffer was constructed around each sampling coordinate; median values of the 10 m pixels within the neighborhood were extracted to reduce sensitivity to single-pixel noise and geolocation uncertainty. Following spatial harmonization and quality control, the eight MSI bands and physically interpretable derived spectral features were used for Chl-a retrieval. These predictors included band ratios, normalized-difference indices, three-band combinations, and red-edge line-height features designed to characterize Chl-a-related spectral responses in the visible and red-edge regions (Dall'Olmo et al., 2005; Mishra & Mishra, 2012; Gitelson et al., 2008; Gower et al., 2005). These candidate predictors are summarized in Table 2.

Table 2 Candidate spectral predictors and physically interpretable indices derived from Sentinel-2 MSI imagery for Chl-a retrieval

Feature category	Spectral predictor	Formula / bands	Reference
Original reflectance	MSI bands	B2, B3, B4, B5, B6, B7, B8, B8A	European Space Agency (2015)
Band ratio	Red-edge/red ratio	B_5/B_4	Gitelson et al. (2008)
Normalized difference index	NDCI	$\frac{B_5 - B_4}{B_5 + B_4}$	Mishra and Mishra (2012)
Three-band index	3BDA	$(B_4^{-1} - B_5^{-1})B_6$	Dall'Olmo et al. (2005); Gitelson et al. (2008)
Red-edge line-height feature	RE-LH	$B_5 - B_4 - \frac{\lambda_5 - \lambda_4}{\lambda_6 - \lambda_4}(B_6 - B_4)$	Gower et al. (2005), adapted

For UAV hyperspectral imagery, the radiometrically and geometrically corrected mosaics were first subjected to water-body masking to exclude land, shoreline, and other invalid pixels. The water mask was generated from NDWI using (R560 − R840)/(|R560| + |R840| + 10^{-8}), with an NDWI threshold of −0.03; the resulting water mask was eroded by two pixels to reduce land–water mixed-edge effects. Shoreline mixed pixels, boats, shadows, and strong-glint areas were further excluded during quality control. Spectral quality control used high-frequency spectral noise and near-infrared noise metrics; observations with an absolute robust z-score > 5 for either metric were excluded. The July–October dataset contained 53 initially matched UAV spectra, of which six spectra from the 18 September UAV-A survey were excluded by this objective spectrum-only quality-control procedure, leaving 47 valid samples. The retained spectra were smoothed using a Savitzky–Golay filter (window length 11, polynomial order 2) and transformed using standard normal variate (SNV) to reduce high-frequency noise and baseline/amplitude variation (Savitzky & Golay, 1964; Barnes et al., 1989). Considering spectral quality and the wavelength range relevant to Chl-a retrieval, wavelengths between 430 and 780 nm were retained as candidate hyperspectral predictors. Field sampling points were overlaid on the UAV hyperspectral imagery, and the mean reflectance within a 3 × 3 pixel window centered on each sampling

point was extracted as the matched UAV spectrum.

The preprocessed Sentinel-2 and UAV spectral observations were subsequently matched with field-measured Chl-a concentrations according to the recorded sampling coordinates. For Sentinel-2, the 15 m neighborhood described above was used with median extraction at 10 m scale; for UAV hyperspectral imagery, the mean reflectance within a 3 × 3 pixel window centered on each sampling point was used. Samples affected by cloud, cloud shadow, land contamination, invalid pixels, or poor spectral quality were excluded during spatial matching and quality control. Separate modelling datasets were constructed for the two remote-sensing platforms because of their distinct spectral and spatial characteristics. After quality control and spatial matching, 150 Sentinel-2–field matched samples and 47 UAV–field matched samples were retained for model development and validation. Field-measured Chl-a concentrations were used directly as the response variable without logarithmic transformation.

Model development

Separate Chl-a retrieval models were developed for Sentinel-2 MSI and UAV hyperspectral observations because of their substantial differences in spectral dimensionality and spatial resolution. For both datasets, field-measured Chl-a concentrations were used directly as the response variable without logarithmic transformation, while the preprocessed spectral variables described in Section 2.3 were used as predictors.

Four regression algorithms were evaluated: partial least squares regression (PLSR), random forest (RF), extreme gradient boosting (XGBoost), and support vector regression (SVR). PLSR was used as a linear latent-variable method capable of handling multicollinearity among spectral predictors (Wold et al., 2001). RF and XGBoost were employed to characterize nonlinear relationships and interactions among spectral variables through ensemble tree-based learning (Breiman, 2001; Chen & Guestrin, 2016), whereas SVR was used as a kernel-based regression approach suitable for high-dimensional datasets with relatively limited sample sizes (Drucker et al., 1996). The four algorithms were applied independently to the Sentinel-2 and UAV datasets.

Given the limited number of field-matched samples, leave-one-out cross-validation (LOOCV) was adopted as the primary sample-wise evaluation scheme (Arlot & Celisse, 2010). The four-model

comparison used fixed model configurations established from the model-tuning procedure summarized in Supplementary Table S1. To provide an additional check on hyperparameter-selection uncertainty for the selected UAV model, the final UAV-SVR was also evaluated using nested LOOCV, with an outer leave-one-out loop and an inner three-fold cross-validation grid search. The inner grid searched C = {30, 100, 300}, gamma = {scale, 0.001, 0.003, 0.01}, and epsilon = {0.5, 1.0}. Hyperparameter selection in the nested procedure was performed only within the corresponding outer training subset. The nested UAV-SVR yielded an R^2 of 0.807, an RMSE of 4.71 μg L^{-1}, and an MAE of 3.81 μg L^{-1}, closely confirming the primary LOOCV result. The selected models were subsequently applied to the corresponding imagery for spatial Chl-a mapping.

Model evaluation and spatial mapping

Model performance was quantitatively evaluated using the coefficient of determination ($\boldsymbol{R^2}$), root mean square error (RMSE), and mean absolute error (MAE). These metrics were calculated from the cross-validated predictions obtained for each model:

$$\boldsymbol{R^2 = 1 - \frac{\sum_{i=1}^{n}(y_i - \hat{y}_i)^2}{\sum_{i=1}^{n}(y_i - \bar{y})^2}}$$

$$\boldsymbol{RMSE = \sqrt{\frac{1}{n}\sum_{i=1}^{n}(y_i - \hat{y}_i)^2}}$$

$$\boldsymbol{MAE = \frac{1}{n}\sum_{i=1}^{n}|y_i - \hat{y}_i|}$$

where $\boldsymbol{y_i}$ and $\boldsymbol{\hat{y}_i}$ represent the measured and predicted Chl-a concentrations for sample $\boldsymbol{i}$, respectively; $\boldsymbol{\bar{y}}$ is the mean measured Chl-a concentration; and $\boldsymbol{n}$ is the number of samples. Higher $\boldsymbol{R^2}$ values together with lower RMSE and MAE values indicate better predictive performance. In addition, measured-versus-predicted scatter plots and the distribution of predictions relative to the 1:1 line were examined to identify potential systematic overestimation or underestimation.

For each remote-sensing platform, the best-performing model was subsequently applied pixel by pixel to the corresponding preprocessed imagery to generate spatially continuous Chl-a maps. Sentinel-2 imagery was used to characterize the reservoir-wide distribution of Chl-a on a common 10 m grid, whereas UAV hyperspectral imagery was used to resolve fine-scale Chl-a variability within the two representative local survey areas. Only valid water pixels retained after cloud, cloud-shadow, land, and

invalid-pixel masking were included in the Sentinel-2 mapping.

Because Sentinel-2 and UAV observations differed substantially in spatial resolution and spectral characteristics, the resulting products were not directly fused at the pixel level. Instead, the two datasets were interpreted according to their respective observation scales: Sentinel-2 provided the reservoir-scale spatial context, while UAV-derived maps were used to characterize finer spatial gradients and local heterogeneity within representative areas. For cloud-affected Sentinel-2 scenes, UAV observations over the corresponding local waters were additionally examined as supplementary information where valid satellite retrievals were unavailable.

Results and Discussion

In situ Chl-a conditions

Five field campaigns conducted from July to October 2025 revealed clear temporal and spatial variations in Chl-a concentrations in Mianhuatan Reservoir. Across all observations, Chl-a concentrations ranged from 11 to 62 μg L^{-1}. The highest mean concentration was observed on 1 July, reaching 49.87 μg L^{-1}, with a relatively narrow range of 42–62 μg L^{-1} and a coefficient of variation (CV) of 9.22%, indicating relatively limited spatial variability among sampling sites. Chl-a concentrations subsequently decreased, with mean values of 36.42 and 34.45 μg L^{-1} on 23 and 28 August, respectively. The wider concentration range on 23 August (20–60 μg L^{-1}) and the higher CV of 28.24% indicated more pronounced spatial differences among sampling locations. The temporal distribution of Chl-a concentrations across the five sampling campaigns is shown in Fig. 3, and the corresponding descriptive statistics are summarized in Table 3.

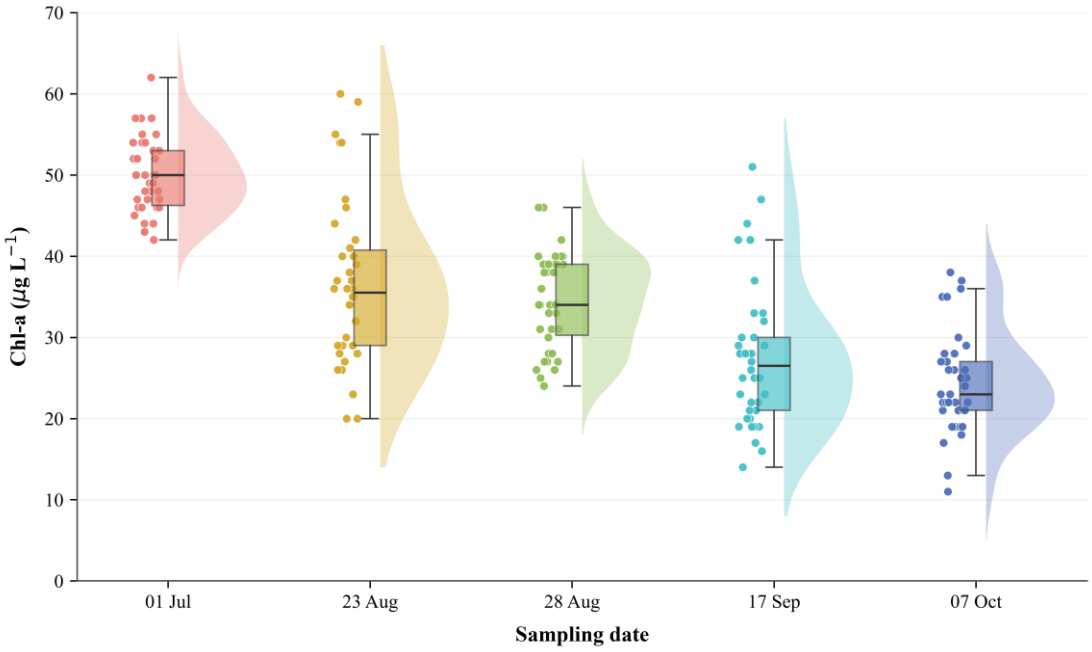


Fig. 3 Variability of in situ Chl-a concentrations across sampling dates

Table 3 Descriptive statistics of in situ chlorophyll-a concentrations across sampling dates

Sampling Time	Min	Max	Mean	SD	CV (%)
1 July 2025	42	62	49.87	4.6	9.22
23 August 2025	20	60	36.42	10.29	28.24
28 August 2025	24	46	34.45	5.84	16.96
17 September 2025	14	51	27.42	8.77	31.99
7 October 2025	11	38	24.26	6.18	25.49

Chl-a concentrations further declined in September and October, with mean values of 27.42 μg L^{-1} on 17 September and 24.26 μg L^{-1} on 7 October. The concentration range on 17 September was 14–51 μg L^{-1}, and the CV reached 31.99%, the highest among the five campaigns, indicating substantial spatial heterogeneity within the reservoir. Overall, Chl-a showed a general decreasing trend from July to October, while considerable spatial variability remained during several sampling campaigns. These variations provided an appropriate concentration gradient for subsequent Chl-a retrieval modeling and spatial mapping using Sentinel-2 and UAV observations.

Performance of Chl-a retrieval models

To compare the capability of different algorithms for Chl-a retrieval, RF, SVR, XGBoost, and PLSR models were developed separately using UAV hyperspectral data and Sentinel-2 multispectral data. Model performance was evaluated using the coefficient of determination (R^2), root mean square error

(RMSE), and mean absolute error (MAE) from cross-validated predictions (Figs. 4 and 5; Table 4). Overall, the four models captured the general variability in measured Chl-a concentrations to different degrees, with clear differences in predictive performance between the two remote-sensing platforms.

For the UAV dataset, SVR achieved the best predictive performance, with $R^2 = 0.81$, RMSE = 4.72 μg L^{-1}, and MAE = 3.79 μg L^{-1} (Fig. 4; Table 4). A nested LOOCV applied to the final UAV-SVR model yielded $R^2 = 0.807$, RMSE = 4.71 μg L^{-1}, and MAE = 3.81 μg L^{-1}, indicating that the model performance was stable after accounting for hyperparameter selection within the training data. PLSR showed the second-best performance ($R^2 = 0.70$, RMSE = 5.84 μg L^{-1}, MAE = 4.71 μg L^{-1}), while RF produced comparable results ($R^2 = 0.68$, RMSE = 6.07 μg L^{-1}, MAE = 4.53 μg L^{-1}). XGBoost showed relatively lower performance ($R^2 = 0.62$, RMSE = 6.66 μg L^{-1}, MAE = 5.00 μg L^{-1}). The scatter plots indicate that all models generally reproduced the variation in the intermediate Chl-a range, whereas some underestimation occurred at higher concentrations. SVR showed the lowest overall dispersion around the 1:1 line and was therefore selected as the optimal model for UAV-based Chl-a mapping.

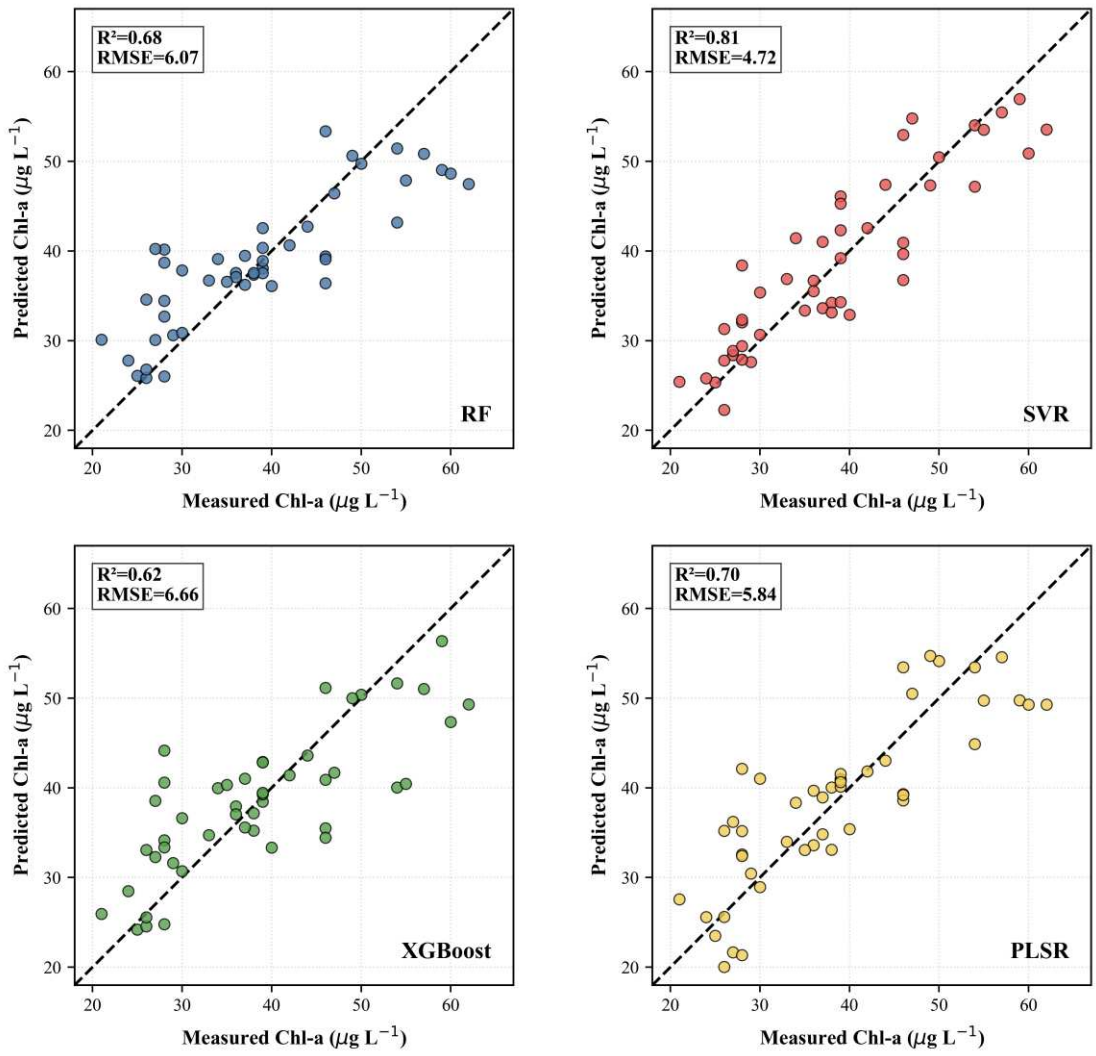


Fig. 4 Performance of UAV-based Chl-a retrieval models. Comparison between measured and predicted Chl-a concentrations for RF, SVR, XGBoost, and PLSR models. The dashed line represents the 1:1 reference line

For the Sentinel-2 dataset, XGBoost achieved the highest predictive accuracy, with R^2 = 0.65, RMSE = 5.93 μg L^{-1}, and MAE = 4.42 μg L^{-1} (Fig. 5; Table 4). RF and SVR showed similar performance, with R^2 values of 0.59 and 0.60, RMSE values of 6.35 and 6.34 μg L^{-1}, and MAE values of 4.62 and 4.82 μg L^{-1}, respectively. PLSR showed the lowest predictive performance (R^2 = 0.47, RMSE = 7.22 μg L^{-1}, MAE = 5.25 μg L^{-1}). Although RF, SVR, and XGBoost generally reproduced the overall trend in measured Chl-a concentrations, some underestimation was evident for high-concentration samples. XGBoost predictions were comparatively more concentrated around the 1:1 line, indicating better overall agreement with field measurements. XGBoost was therefore selected as the optimal Sentinel-2 Chl-a retrieval model.

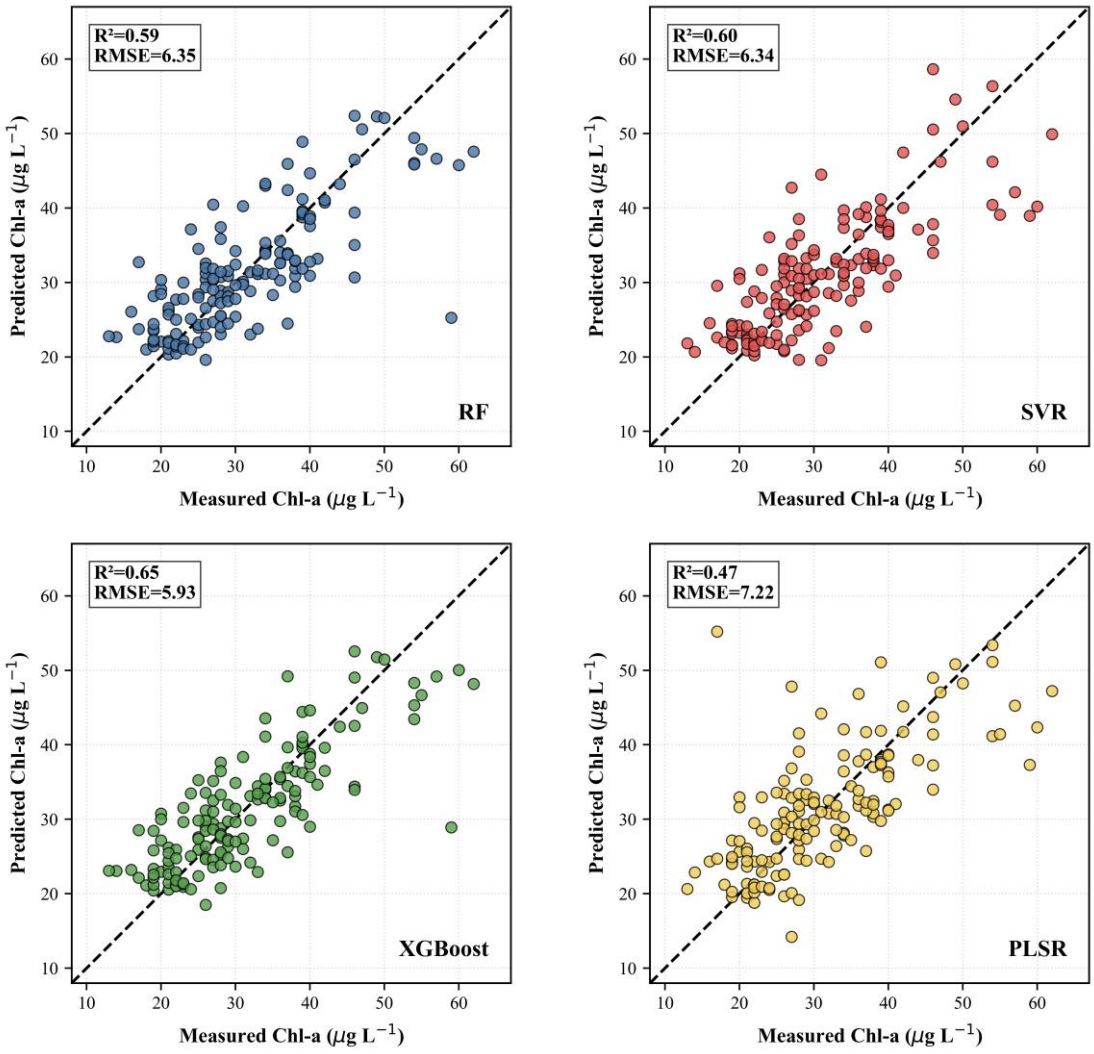


Fig. 5 Performance of Sentinel-2-based Chl-a retrieval models. Comparison between measured and predicted Chl-a concentrations for RF, SVR, XGBoost, and PLSR models. The dashed line represents the 1:1 reference line

Overall, the optimal models differed between the two remote-sensing platforms. SVR performed best for the UAV dataset, whereas XGBoost provided the best performance for Sentinel-2. These results suggest that the statistical relationships between spectral information and Chl-a vary between data sources, requiring platform-specific model selection. The selected SVR and XGBoost models were subsequently applied to generate local high-resolution UAV Chl-a maps and reservoir-scale Sentinel-2 Chl-a distributions, respectively.

Table 4 Performance of Chl-a retrieval models based on cross-validated predictions

Platform	Model	R^2	RMSE (μg L^{-1})	MAE (μg L^{-1})
UAV	RF	0.680	6.07	4.53
UAV	SVR	0.807	4.71	3.81

UAV	XGBoost	0.615	6.66	5.00
UAV	PLSR	0.704	5.84	4.71
Sentinel-2	RF	0.594	6.35	4.62
Sentinel-2	SVR	0.595	6.34	4.82
Sentinel-2	XGBoost	0.646	5.93	4.42
Sentinel-2	PLSR	0.474	7.22	5.25

Reservoir-scale background from Sentinel-2 and local fine-scale characterization by UAV

Based on the best-performing retrieval models described above, Chl-a distributions were mapped at different spatial scales using Sentinel-2 and UAV imagery (Fig. 6). The Sentinel-2 retrieval provided a reservoir-wide spatial background of Chl-a across Mianhuatan Reservoir [Fig. 6(a)]. Overall, pronounced spatial heterogeneity was observed throughout the reservoir, with mapped Chl-a concentrations of approximately 15–60 μg L^{-1}. Clear differences were evident among different reservoir sections. Relatively high Chl-a concentrations occurred in several upstream branches and parts of the central reservoir, whereas medium to lower concentrations were more common in the southern and relatively open-water areas. Sentinel-2 therefore captured the overall spatial pattern of Chl-a at the reservoir scale and provided the spatial context for subsequent detailed UAV observations.

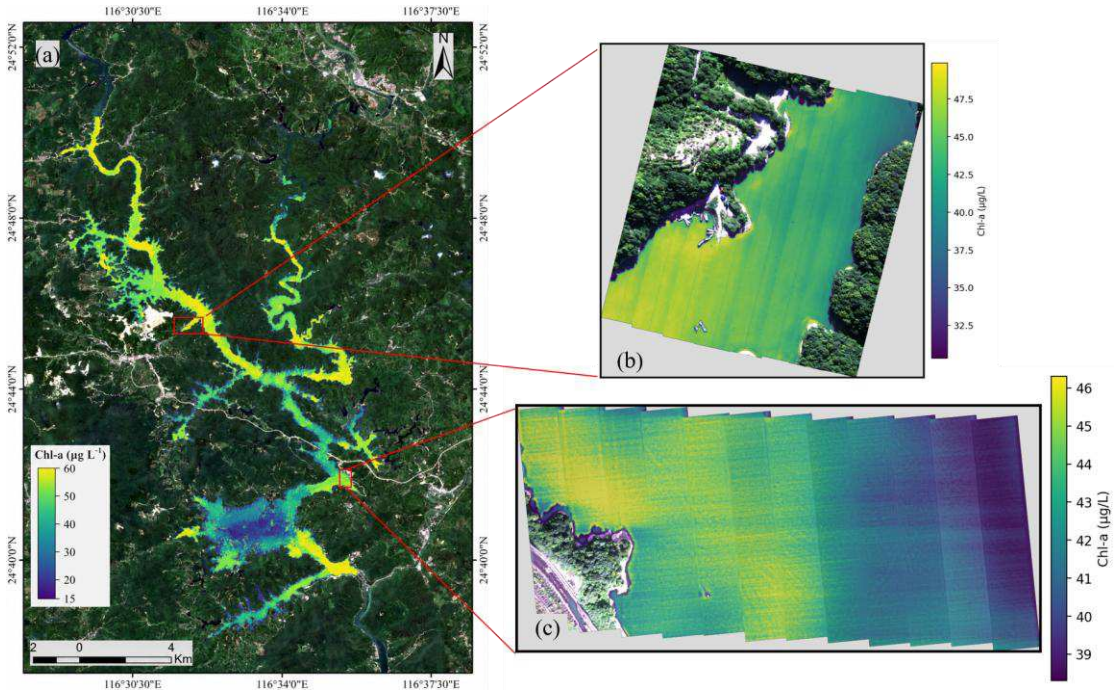


Fig. 6 Cross-scale Chl-a distributions derived from Sentinel-2 and UAV observations on 23 August 2025. (a) Reservoir-wide Chl-a distribution derived from Sentinel-2; (b,c) fine-scale UAV-derived Chl-a distributions in two representative local areas surveyed on the same day

Within this reservoir-scale context, two local areas were further characterized using UAV

hyperspectral imagery [Fig. 6(b,c)]. In Area 1, UAV-derived Chl-a concentrations ranged approximately from 30 to 50 μg L^{-1}, with a clear and continuous spatial gradient across the water body [Fig. 6(b)]. Relatively high concentrations were mainly distributed in the lower-left and central portions of the area and gradually decreased toward the upper-right. In Area 2, Chl-a concentrations were approximately 38.5–46.0 μg L^{-1} [Fig. 6(c)]. A similarly distinct directional pattern was observed, with relatively higher concentrations on the left side and progressively lower values toward the right. Compared with the more generalized representation provided by Sentinel-2 at the reservoir scale, the UAV-derived maps revealed more continuous concentration transitions and finer-scale spatial structures within the local water bodies.

Quantitative cross-scale comparison at representative local footprints

To complement the visual comparison of spatial patterns, mean Chl-a concentrations were compared within the same representative local footprints without performing pixel-level fusion or treating one platform as a validation reference for the other. For Area 1, the UAV-derived local product had a mean Chl-a concentration of 45.00 μg L^{-1} across 597 pixels, compared with 39.62 μg L^{-1} from the corresponding Sentinel-2 representation, giving an absolute difference of 5.38 μg L^{-1} and a relative difference of 13.59%. For Area 2, the corresponding means were 33.50 μg L^{-1} for UAV and 36.57 μg L^{-1} for Sentinel-2 across 1,575 pixels, with an absolute difference of −3.07 μg L^{-1} and a relative difference of −8.39%. The relatively small differences in footprint means, together with the finer continuous gradients resolved by UAV imagery, indicate that the two platforms provide broadly comparable local concentration context while representing spatial variability at different observational scales. The quantitative footprint-level comparison is summarized in Table 5.

Table 5 Quantitative comparison of Chl-a means within representative local footprints on 23 August 2025

Area	n (UAV pixels)	UAV mean (μg L^{-1})	Sentinel-2 mean (μg L^{-1})	Difference (μg L^{-1})	Relative difference (%)
Area 1	597	45.00	39.62	5.38	13.59
Area 2	1,575	33.50	36.57	−3.07	−8.39

Taken together, the retrieval results at different spatial scales demonstrate clear cross-scale complementarity between Sentinel-2 and UAV observations. Sentinel-2 provided the reservoir-wide spatial background, allowing broad differences among reservoir sections to be identified, whereas UAV observations enabled fine-scale characterization of local areas and further revealed local concentration gradients and spatial heterogeneity that were less apparent at the satellite scale. The integration of the

two platforms therefore enabled cross-scale characterization of Chl-a from the whole-reservoir pattern to detailed local spatial structures.

Supplementary UAV observations under partial cloud cover

In addition to differences in spatial resolution, partial cloud cover represented an important constraint on the spatial completeness of Sentinel-2 water-quality observations. On 17 September 2025, local clouds and cloud shadows affected several portions of Mianhuatan Reservoir during the Sentinel-2 overpass [Fig. 7(a)]. The selected UAV survey area was also subject to limited local cloud influence. After cloud and invalid-pixel screening, Sentinel-2 still provided Chl-a information over most cloud-free waters; however, some pixels within and around the target area were affected by cloud and cloud-shadow contamination, reducing the spatial continuity of the satellite-derived Chl-a distribution [Fig. 7(b)].

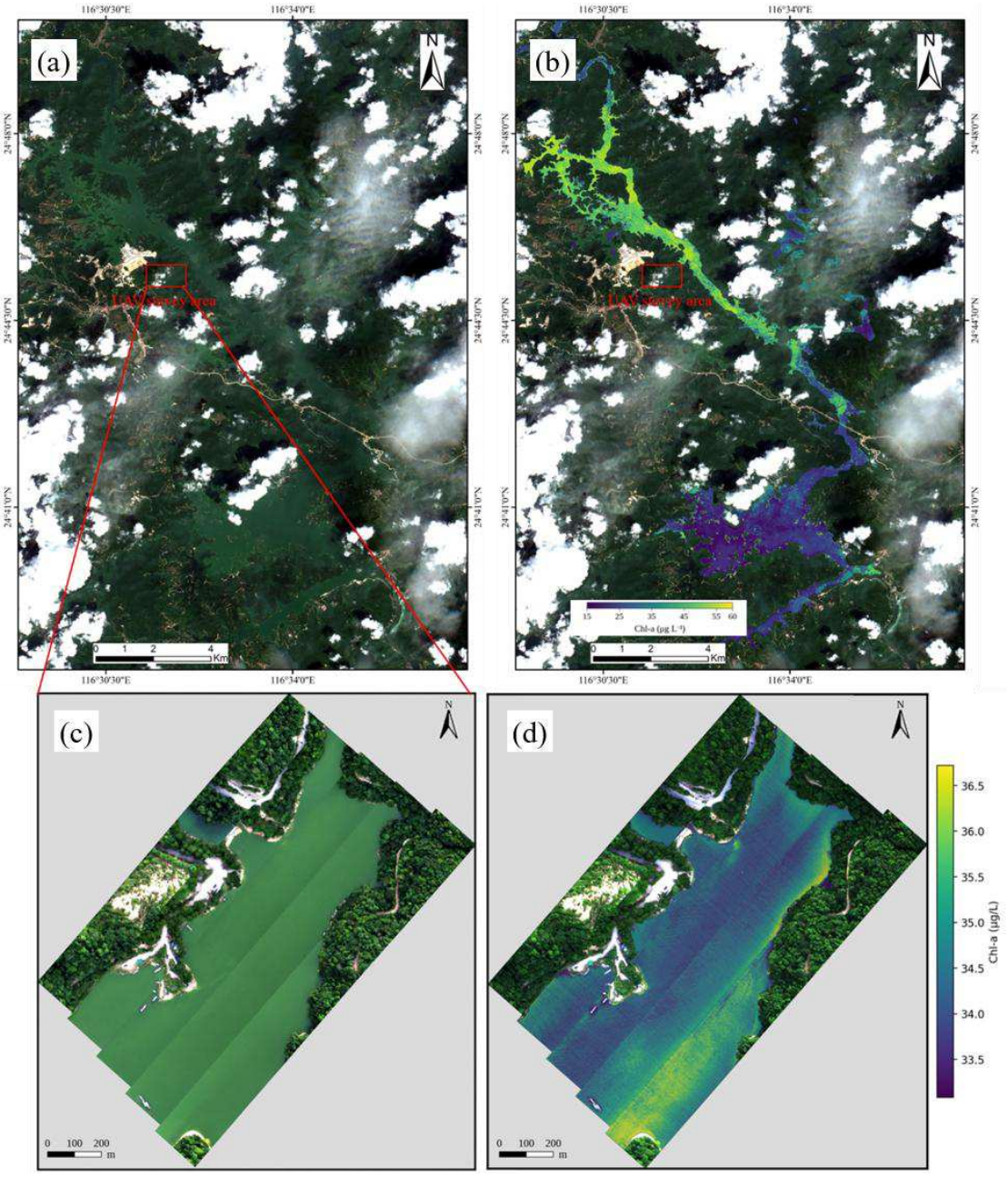


Fig. 7 Supplementary UAV observations under partial cloud-cover conditions on 17 September 2025. (a) Sentinel-2 true-color image showing local cloud contamination over Mianhuatan Reservoir and the location of the UAV survey area; (b) Sentinel-2-derived Chl-a distribution over valid cloud-free water pixels; (c) true-color UAV image acquired on the same day over the selected local survey area; and (d) UAV-derived high-resolution Chl-a distribution for the corresponding water body

In contrast, the UAV survey conducted on the same day provided nearly complete high-resolution image coverage of the selected local water body [Fig. 7(c)]. UAV-derived Chl-a concentrations ranged approximately from 33.5 to 36.5 μg L^{-1} and exhibited a spatially continuous distribution within the survey area [Fig. 7(d)]. The UAV observations therefore provided continuous local-scale Chl-a information where the corresponding Sentinel-2 representation was partially affected by cloud

contamination.

These results further demonstrate the complementary roles of satellite and UAV observations under varying observation conditions. Sentinel-2 retained broad spatial coverage across cloud-free portions of the reservoir, whereas UAV observations provided targeted, spatially continuous information at the local scale. Under partial cloud-cover conditions, UAV observations thus served not as a replacement for satellite monitoring or as a means of reconstructing missing satellite pixels, but as an independent supplementary source of high-resolution Chl-a information that improved the completeness of local water-quality characterization.

Cross-scale complementarity of Sentinel-2 and UAV observations

The principal value of the Sentinel-2–UAV framework developed in this study lies not simply in combining two remote-sensing platforms, but in assigning complementary observational roles to sensors operating at distinctly different spatial scales. Sentinel-2 provides synoptic coverage of the entire reservoir and is therefore suitable for identifying broad spatial differences in Chl-a among different reservoir sections. In contrast, UAV hyperspectral imagery provides centimeter-scale observations over targeted local areas, allowing continuous concentration gradients and fine-scale spatial heterogeneity to be resolved within representative waters. The two platforms therefore address different but closely connected monitoring questions: Sentinel-2 characterizes the reservoir-wide spatial context, whereas UAV observations refine the spatial structure within selected local waters.

This cross-scale distinction was clearly reflected in the spatial mapping results. Sentinel-2 revealed pronounced differences in Chl-a across Mianhuatan Reservoir, with relatively high concentrations occurring in several upstream branches and parts of the central reservoir, whereas medium to lower concentrations were more common in the southern and relatively open-water areas. Within this reservoir-scale background, UAV observations further resolved continuous local Chl-a gradients in the two representative survey areas that were less apparent at the satellite scale. These differences indicate that the spatial patterns observed from satellite imagery are influenced not only by actual water-quality variability but also by the spatial support and averaging characteristics of the sensor. Consequently, a relatively smooth satellite-derived Chl-a distribution should not necessarily be interpreted as spatial uniformity of the water body.

The footprint-level comparison further supports this scale-dependent interpretation. The relative differences between UAV and Sentinel-2 mean Chl-a were 13.59% in Area 1 and −8.39% in Area 2, indicating that the platforms retained similar local concentration context despite differences in spatial support. At the same time, UAV imagery preserved continuous within-footprint gradients that are less apparent in the coarser satellite representation. These results support the use of Sentinel-2 for reservoir-wide screening and UAV observations for targeted local characterization, rather than direct pixel-level fusion.

The complementary roles of Sentinel-2 and UAV observations are particularly relevant for canyon-type reservoirs such as Mianhuatan Reservoir. The study area contains open main-reservoir waters, nearshore zones, tributary arms, and semi-enclosed bays, forming a morphologically complex aquatic environment. Under such conditions, a single observation scale is unlikely to capture both broad reservoir-wide patterns and localized fine-scale variability. Satellite imagery provides the spatial continuity required for reservoir-scale assessment, but its pixel size may smooth or obscure small-scale gradients near shorelines, tributary junctions, and narrow water bodies. UAV imagery, by contrast, can characterize these local structures in much greater detail, although its limited flight endurance and survey extent make routine full-reservoir coverage impractical. Their coordinated use therefore provides a practical means of linking broad spatial patterns with targeted local observations.

Importantly, the framework proposed in this study should not be interpreted as direct pixel-level fusion between Sentinel-2 and UAV products. The two datasets differ substantially in spatial resolution, spectral configuration, and spatial support, and were therefore modelled independently. Instead, their integration is functional and hierarchical. Sentinel-2 provides the reservoir-scale spatial background and can be used to identify broad Chl-a patterns and areas requiring further attention, whereas UAV surveys can subsequently focus on representative or environmentally sensitive waters to resolve finer spatial structures. This hierarchical strategy reduces the need for exhaustive high-resolution UAV coverage while retaining the ability to investigate local heterogeneity where additional spatial detail is required.

Overall, the Sentinel-2–UAV framework establishes a clear division of observational roles across spatial scales. Sentinel-2 is primarily used to identify where large-scale Chl-a differences occur across the reservoir, whereas UAV observations provide information on how Chl-a varies within selected local waters. This functional coordination links reservoir-wide spatial context with local fine-scale

493 characterization and provides a more complete representation of Chl-a variability than either platform
494 alone. The value of the framework therefore lies not in replacing one platform with another, but in
495 combining their respective strengths to support multi-scale water-quality monitoring in morphologically
496 complex reservoirs.

497 Supplementary value of UAV observations under incomplete satellite coverage

498 Cloud and cloud-shadow contamination remains an important limitation of optical satellite remote
499 sensing for inland-water monitoring, particularly when water-quality information is required for a
500 specific observation date. In this study, Sentinel-2 retained broad spatial coverage over cloud-free
501 portions of Mianhuatan Reservoir, but partial cloud contamination resulted in local gaps in valid Chl-a
502 retrievals within the target area. In contrast, UAV observations over the corresponding local waters
503 provided spatially continuous local-scale Chl-a information, demonstrating their value as a
504 supplementary observation source when satellite retrievals are spatially incomplete.

505 The value of this supplementary capability arises from the different acquisition characteristics of
506 satellite and UAV platforms. Sentinel-2 operates according to a fixed orbital schedule, meaning that the
507 availability of usable imagery depends not only on revisit frequency but also on atmospheric conditions
508 at the time of overpass. Even when most of a reservoir is cloud free, local cloud or cloud-shadow
509 contamination may still obscure tributary arms, nearshore waters, or other areas of interest. UAV surveys,
510 by contrast, can be scheduled more flexibly within suitable local weather windows and directed toward
511 specific target waters. This flexibility makes UAV observations particularly useful for localized follow-
512 up monitoring when a satellite scene does not provide complete spatial information.

513 The cloud-affected case observed in Mianhuatan Reservoir illustrates this operational difference.
514 Although Sentinel-2 provided valid Chl-a retrievals over most cloud-free waters, parts of the selected
515 target area lacked usable satellite information after cloud and invalid-pixel screening. The corresponding
516 UAV survey nevertheless produced a continuous local Chl-a distribution, allowing the spatial variability
517 of the target water body to remain observable. This suggests that the practical value of UAV observations
518 extends beyond their finer spatial resolution. Their ability to provide targeted observations at user-defined
519 locations and times can also improve the spatial completeness and adaptability of water-quality
520 monitoring under variable observation conditions. Similar advantages of UAV observations under cloud-

affected satellite conditions have also been emphasized in previous multi-platform monitoring studies.

Importantly, this supplementary role should not be interpreted as reconstruction of cloud-contaminated Sentinel-2 pixels or as a replacement for satellite monitoring. Sentinel-2 and UAV observations were independently processed and modelled in this study, and no pixel-level gap filling or direct image fusion was performed. UAV-derived Chl-a maps therefore represent independent local observations rather than estimates of missing satellite pixels. Sentinel-2 remains essential for characterizing reservoir-wide spatial patterns, while UAV observations provide additional information for specific local waters where valid satellite retrievals are temporarily unavailable. The two platforms therefore remain complementary rather than interchangeable. From an operational perspective, this supplementary capability further strengthens the cross-scale Sentinel-2–UAV framework. Under favorable observation conditions, Sentinel-2 can provide efficient reservoir-wide screening and identify areas requiring closer examination. When valid satellite information is locally incomplete, UAV surveys can be directed toward these areas to maintain detailed local observations. Such a strategy avoids the need for exhaustive UAV coverage of the entire reservoir while retaining the ability to acquire high-resolution information where and when it is most needed. For morphologically complex reservoirs such as Mianhuatan Reservoir, this coordinated observation strategy provides a practical means of improving the completeness and flexibility of Chl-a monitoring across different environmental and observation conditions.

Limitations and future perspectives

Several limitations of the present study should be acknowledged. First, the proposed Sentinel-2–UAV framework was developed and evaluated in a single canyon-type reservoir, and all field campaigns were conducted between July and October 2025. Although the five campaigns captured clear temporal and spatial variations in Chl-a, the current dataset does not fully represent other hydrological periods, seasonal conditions, or reservoirs with different trophic states and optical properties. LOOCV and nested LOOCV were used to assess sample-wise and hyperparameter-selection uncertainty, respectively, but independent temporal or spatial validation was not available. The transferability of the retrieval models and the broader applicability of the cross-scale monitoring framework therefore require further evaluation using independent observations from other seasons and water bodies.

Second, UAV observations were limited to two representative local survey areas, and only 47 UAV–field matched samples were retained after spatial matching and quality control. These observations were sufficient to demonstrate the capability of UAV hyperspectral imagery to resolve fine-scale Chl-a variability, but they cannot represent all local environmental conditions across the entire reservoir. Expanding UAV surveys to additional tributary arms, nearshore zones, semi-enclosed bays, and other hydrodynamically distinct areas would help evaluate the consistency of local-scale Chl-a patterns across a broader range of reservoir environments.

Third, the present framework emphasizes functional coordination across spatial scales rather than direct multi-source data fusion. Sentinel-2 and UAV observations were independently processed, modelled, and interpreted, and their Chl-a products differ substantially in spatial resolution, spectral configuration, and spatial support. Future work could explore more rigorous cross-scale linkage strategies, including spatial aggregation, scale-transfer modelling, and hierarchical data-assimilation approaches, while explicitly accounting for the large difference in spatial resolution between satellite and UAV observations.

Finally, the current study focused exclusively on Chl-a as the target water-quality variable. Future applications could incorporate additional remotely retrievable parameters, such as suspended solids and turbidity, together with field-measured nutrient indicators where appropriate. Extending the framework toward multi-parameter water-quality assessment would provide a more comprehensive basis for reservoir monitoring and management.

Overall, these limitations define the current scope of the proposed framework and provide clear directions for further development. Broader seasonal coverage, independent validation, expanded UAV observations, and more explicit cross-scale linkage will be important for evaluating its robustness and transferability to other reservoir systems.

Conclusions

This study developed a cross-scale Sentinel-2–UAV framework for chlorophyll-a (Chl-a) monitoring in Mianhuatan Reservoir by coordinating reservoir-wide satellite observations with targeted high-resolution UAV surveys. Field-measured Chl-a concentrations were used as reference data, while Sentinel-2 MSI and UAV hyperspectral imagery were modelled independently according to their

respective spectral and spatial characteristics.

The results demonstrated clear functional complementarity between the two platforms. Sentinel-2 provided the reservoir-wide spatial background, whereas UAV hyperspectral imagery resolved continuous concentration gradients and finer spatial heterogeneity within representative local waters. The optimal UAV-SVR model achieved R^2 = 0.81, RMSE = 4.72 μg L^{-1}, and MAE = 3.79 μg L^{-1} in the primary model comparison, while the nested LOOCV confirmation yielded R^2 = 0.807, RMSE = 4.71 μg L^{-1}, and MAE = 3.81 μg L^{-1}. The Sentinel-2-XGBoost model achieved R^2 = 0.65, RMSE = 5.93 μg L^{-1}, and MAE = 4.42 μg L^{-1}. Quantitative footprint comparisons further showed relative differences of 13.59% and −8.39% between UAV and Sentinel-2 mean Chl-a in the two representative areas, supporting their complementary rather than interchangeable observational roles.

The framework also showed supplementary value under partial cloud-cover conditions. When local cloud and cloud-shadow contamination reduced the spatial continuity of valid Sentinel-2 retrievals, same-day UAV observations provided spatially continuous high-resolution Chl-a information within the selected local area. This role should be regarded as supplementary rather than substitutive: UAV observations were not used to reconstruct missing satellite pixels, but instead provided independent local-scale information where satellite observations were spatially incomplete.

Overall, the proposed framework links reservoir-wide spatial context with local fine-scale characterization without requiring direct pixel-level fusion between Sentinel-2 and UAV products. The results demonstrate the potential of coordinated satellite–UAV observations for multi-scale Chl-a monitoring in morphologically complex reservoirs. Future work should extend the framework across additional seasons and reservoir types, incorporate independent validation datasets, expand UAV observations to a wider range of local environments, and investigate more explicit cross-scale linkage and multi-parameter water-quality monitoring approaches.

Statements and Declarations

Author contributions

Miaohua Zhong: Conceptualization, methodology, software, validation, formal analysis, investigation,

data curation, visualization, and writing—original draft. Chaojun Lin: Methodology, formal analysis, data curation, validation, and writing—review and editing. Xuewen Chen: Investigation, data curation, validation, and visualization. Lvxin Qian: Investigation, data curation, validation, and visualization. Qiuting Zhang: Investigation, field coordination, data acquisition, and data curation. Fan Zhang: Investigation, field coordination, data acquisition, and data curation. Kaixin Qiu: Investigation, field coordination, data acquisition, and data curation. Wenbin Pan: Conceptualization, supervision, project administration, funding acquisition, and writing—review and editing. All authors read and approved the final manuscript.

Competing interests

The authors declare no competing interests.

Funding

This research was supported by the Fujian Provincial Department of Science and Technology through the Fujian Provincial Science and Technology Plan Project "Research on Water Ecological Restoration and Algal Bloom Early-Warning Monitoring Technology for Mianhuatan Reservoir" (No. 2024Y61010228).

Data availability

The Sentinel-2 imagery used in this study is publicly available through the Google Earth Engine platform. The field-measured chlorophyll-a data, UAV hyperspectral data, and derived datasets generated and/or analyzed during the current study are available from the corresponding author on reasonable request.

Ethical responsibilities of Authors

All authors have read, understood, and have complied as applicable with the statement on "Ethical responsibilities of Authors" as found in the Instructions for Authors

References

Arlot, S., & Celisse, A. (2010). A survey of cross-validation procedures for model selection. *Statistics Surveys, 4*, 40–79. https://doi.org/10.1214/09-SS054

Barnes, R. J., Dhanoa, M. S., & Lister, S. J. (1989). Standard normal variate transformation and de-trending of near-infrared diffuse reflectance spectra. *Applied Spectroscopy, 43*, 772–777. https://doi.org/10.1366/0003702894202201

633 Breiman, L. (2001). Random forests. *Machine Learning, 45*, 5–32.
634 https://doi.org/10.1023/A:1010933404324

635 Carlson, R. E. (1977). A trophic state index for lakes. *Limnology and Oceanography, 22*, 361–369.
636 https://doi.org/10.4319/lo.1977.22.2.0361

637 Cawley, G. C., & Talbot, N. L. C. (2010). On over-fitting in model selection and subsequent selection
638 bias in performance evaluation. *Journal of Machine Learning Research, 11*, 2079–2107.

639 Chen, T., & Guestrin, C. (2016). XGBoost: A scalable tree boosting system. *Proceedings of the 22nd*
640 *ACM SIGKDD International Conference on Knowledge Discovery and Data Mining* (pp. 785–
641 794). https://doi.org/10.1145/2939672.2939785

642 Cheng, Y., Mu, Z., Wang, H., Zhao, F., Li, Y., & Lin, L. (2019). Water residence time in a typical
643 tributary bay of the three gorges reservoir. *Water, 11*, 1585. https://doi.org/10.3390/w11081585

644 Cillero Castro, C., Domínguez Gómez, J. A., Delgado Martín, J., Hinojo Sánchez, B. A., Cereijo
645 Arango, J. L., Cheda Tuya, F. A., & Díaz-Varela, R. (2020). An UAV and satellite
646 multispectral data approach to monitor water quality in small reservoirs. *Remote Sensing, 12*,
647 1514. https://doi.org/10.3390/rs12091514

648 Dall'Olmo, G., Gitelson, A. A., Rundquist, D. C., Leavitt, B., Barrow, T., & Holz, J. C. (2005).
649 Assessing the potential of SeaWiFS and MODIS for estimating chlorophyll concentration in
650 turbid productive waters using red and near-infrared bands. *Remote Sensing of Environment,*
651 *96*, 176–187. https://doi.org/10.1016/j.rse.2005.02.007

652 Dronova, I., Kislik, C., Dinh, Z., & Kelly, M. (2021). A review of unoccupied aerial vehicle use in
653 wetland applications: Emerging opportunities in approach, technology, and data. *Drones, 5*,
654 45. https://doi.org/10.3390/drones5020045

655 Drucker, H., Burges, C. J. C., Kaufman, L., Smola, A. J., & Vapnik, V. (1996). Support vector
656 regression machines. In *Advances in Neural Information Processing Systems 9* (pp. 155–161).

657 Drusch, M., Del Bello, U., Carlier, S., Colin, O., Fernandez, V., Gascon, F., Hoersch, B., Isola, C.,
658 Laberinti, P., Martimort, P., Meygret, A., Spoto, F., Sy, O., Marchese, F., & Bargellini, P.
659 (2012). Sentinel-2: ESA's optical high-resolution mission for GMES operational services.

Remote Sensing of Environment, 120, 25–36. https://doi.org/10.1016/j.rse.2011.11.026

European Space Agency (2015). *Sentinel-2 user handbook, issue 1, revision 2*. European Space Agency.

Gai, Y., Yu, D., Zhou, Y., Yang, L., Chen, C., & Chen, J. (2020). An improved model for chlorophyll-a concentration retrieval in coastal waters based on UAV-Borne hyperspectral imagery: A case study in Qingdao, China. *Water, 12*, 2769. https://doi.org/10.3390/w12102769

Gholizadeh, M. H., Melesse, A. M., & Reddi, L. (2016). A comprehensive review on water quality parameters estimation using remote sensing techniques. *Sensors, 16*, 1298. https://doi.org/10.3390/s16081298

Gitelson, A. A., Dall'Olmo, G., Moses, W., Rundquist, D. C., Barrow, T., Fisher, T. R., Gurlin, D., & Holz, J. (2008). A simple semi-analytical model for remote estimation of chlorophyll-a in turbid waters: Validation. *Remote Sensing of Environment, 112*, 3582–3593. https://doi.org/10.1016/j.rse.2008.04.015

Gorelick, N., Hancher, M., Dixon, M., Ilyushchenko, S., Thau, D., & Moore, R. (2017). Google earth engine: Planetary-scale geospatial analysis for everyone. *Remote Sensing of Environment, 202*, 18–27. https://doi.org/10.1016/j.rse.2017.06.031

Gower, J., King, S., Borstad, G., & Brown, L. (2005). Detection of intense plankton blooms using the 709 nm band of the MERIS imaging spectrometer. *International Journal of Remote Sensing, 26*, 2005–2012. https://doi.org/10.1080/01431160500075857

Huang, C., Chen, Y., Zhang, S., & Wu, J. (2018). Detecting, extracting, and monitoring surface water from space using optical sensors: A review. *Reviews of Geophysics, 56*, 333–360. https://doi.org/10.1029/2018RG000598

Kislik, C., Dronova, I., & Kelly, M. (2018). UAVs in support of algal bloom research: A review of current applications and future opportunities. *Drones, 2*, 35. https://doi.org/10.3390/drones2040035

Liu, X., Ho, L., Bruneel, S., & Goethals, P. (2025). Applications of unmanned vehicle systems for multi-spatial scale monitoring and management of aquatic ecosystems: A review. *Ecological*

Informatics, 85, 102926. https://doi.org/10.1016/j.ecoinf.2024.102926

Llodrà-Llabrés, J., Martínez-López, J., Postma, T., Pérez-Martínez, C., & Alcaraz-Segura, D. (2023). Retrieving water chlorophyll-a concentration in inland waters from Sentinel-2 imagery: Review of operability, performance and ways forward. *International Journal of Applied Earth Observation and Geoinformation, 125*, 103605. https://doi.org/10.1016/j.jag.2023.103605

Lu, Q., Si, W., Wei, L., Li, Z., Xia, Z., Ye, S., & Xia, Y. (2021). Retrieval of water quality from UAV-Borne hyperspectral imagery: A comparative study of machine learning algorithms. *Remote Sensing, 13*, 3928. https://doi.org/10.3390/rs13193928

Mamun, M., Hasan, M., & An, K.-G. (2024). Advancing reservoirs water quality parameters estimation using Sentinel-2 and landsat-8 satellite data with machine learning approaches. *Ecological Informatics, 81*, 102608. https://doi.org/10.1016/j.ecoinf.2024.102608

McFeeters, S. K. (1996). The use of the normalized difference water index (NDWI) in the delineation of open water features. *International Journal of Remote Sensing, 17*, 1425–1432. https://doi.org/10.1080/01431169608948714

Miliutina, E., Liu, H., Premsagar, A., Men, J., Su, H., Lu, Y., Palaparthi, A., Mandal, T., Tian, D., & Seo, J. (2026). Flexible high-resolution water quality monitoring and mapping using an autonomous surface vehicle and drone-based multispectral imaging system. *Remote Sensing, 18*, 2473. https://doi.org/10.3390/rs18152473

Ministry of Ecology and Environment of the People's Republic of China (2017). *Water quality—determination of chlorophyll a—spectrophotometric method (hj 897-2017)*. Beijing, China.

Mishra, S., & Mishra, D. R. (2012). Normalized difference chlorophyll index: A novel model for remote estimation of chlorophyll-a concentration in turbid productive waters. *Remote Sensing of Environment, 117*, 394–406. https://doi.org/10.1016/j.rse.2011.10.016

Nguyen, H. Q., Ha, N. T., Nguyen-Ngoc, L., & Pham, T. L. (2021). Comparing the performance of machine learning algorithms for remote and in situ estimations of chlorophyll-a content: A case study in the tri an reservoir, Vietnam. *Water Environment Research, 93*, 2941–2957. https://doi.org/10.1002/wer.1643

Odermatt, D., Gitelson, A., Brando, V. E., & Schaepman, M. (2012). Review of constituent retrieval in optically deep and complex waters from satellite imagery. *Remote Sensing of Environment, 118*, 116–126. https://doi.org/10.1016/j.rse.2011.11.013

Pahlevan, N., Smith, B., Schalles, J., Binding, C., Cao, Z., Ma, R., Alikas, K., Kangro, K., Gurlin, D., Hà, N., Matsushita, B., Moses, W., Greb, S., Lehmann, M. K., Ondrusek, M., Oppelt, N., & Stumpf, R. (2020). Seamless retrievals of chlorophyll-a from Sentinel-2 (MSI) and Sentinel-3 (OLCI) in inland and coastal waters: A machine-learning approach. *Remote Sensing of Environment, 240*, 111604. https://doi.org/10.1016/j.rse.2019.111604

Palmer, S. C. J., Kutser, T., & Hunter, P. D. (2015). Remote sensing of inland waters: Challenges, progress and future directions. *Remote Sensing of Environment, 157*, 1–8. https://doi.org/10.1016/j.rse.2014.09.021

Ryu, J. H. (2022). Uas-based real-time water quality monitoring, sampling, and visualization platform (UASWQP). *HardwareX, 11*, e00277. https://doi.org/10.1016/j.ohx.2022.e00277

Savitzky, A., & Golay, M. J. E. (1964). Smoothing and differentiation of data by simplified least squares procedures. *Analytical Chemistry, 36*, 1627–1639. https://doi.org/10.1021/ac60214a047

Toming, K., Kutser, T., Laas, A., Sepp, M., Paavel, B., & Nõges, T. (2016). First experiences in mapping lake water quality parameters with Sentinel-2 MSI imagery. *Remote Sensing, 8*, 640. https://doi.org/10.3390/rs8080640

Tyler, A. N., Hunter, P. D., Spyrakos, E., Groom, S., Constantinescu, A. M., & Kitchen, J. (2016). Developments in earth observation for the assessment and monitoring of inland, transitional, coastal and shelf-sea waters. *Science of the Total Environment, 572*, 1307–1321. https://doi.org/10.1016/j.scitotenv.2016.01.020

Wang, B., Luo, L., Mei, L., & Zeng, H. (2024). Temporal and spatial distribution of phytoplankton and role of environment factors in the shending river backwater in the Danjiangkou reservoir area. *Water, 16*, 326. https://doi.org/10.3390/w16020326

Warren, M. A., Simis, S. G. H., Martinez-Vicente, V., Poser, K., Bresciani, M., Alikas, K., Spyrakos, E., Giardino, C., & Ansper, A. (2019). Assessment of atmospheric correction algorithms for the

Sentinel-2A multispectral imager over coastal and inland waters. *Remote Sensing of Environment, 225*, 267–289. https://doi.org/10.1016/j.rse.2019.03.018

Wasehun, E. T., Hashemi Beni, L., & Di Vittorio, C. A. (2024). UAV and satellite remote sensing for inland water quality assessments: A literature review. *Environmental Monitoring and Assessment, 196*, 277. https://doi.org/10.1007/s10661-024-12342-6

Wasehun, E. T., Hashemi Beni, L., Di Vittorio, C. A., Zarzar, C. M., & Young, K. R. L. (2025). Comparative analysis of Sentinel-2 and planetscope imagery for chlorophyll-a prediction using machine learning models. *Ecological Informatics, 85*, 102988. https://doi.org/10.1016/j.ecoinf.2024.102988

Wold, S., Sjöström, M., & Eriksson, L. (2001). PLS-regression: A basic tool of chemometrics. *Chemometrics and Intelligent Laboratory Systems, 58*, 109–130. https://doi.org/10.1016/S0169-7439(01)00155-1

Wu, Y., Knudby, A., Pahlevan, N., Lapen, D., & Zeng, C. (2024). Sensor-generic adjacency-effect correction for remote sensing of coastal and inland waters. *Remote Sensing of Environment, 317*, 114433. https://doi.org/10.1016/j.rse.2024.114433

Xiang, R., Wang, L., Li, H., Tian, Z., & Zheng, B. (2021). Water quality variation in tributaries of the three gorges reservoir from 2000 to 2015. *Water Research, 195*, 116993. https://doi.org/10.1016/j.watres.2021.116993

Zhao, Y., He, X., Pan, S., Bai, Y., Wang, D., Li, T., Gong, F., & Zhang, X. (2024). Satellite retrievals of water quality for diverse inland waters from Sentinel-2 images: An example from Zhejiang province, China. *International Journal of Applied Earth Observation and Geoinformation, 132*, 104048. https://doi.org/10.1016/j.jag.2024.104048